



Multi-objective optimization design of bridge piers with hybrid heuristic algorithms*

Francisco J. MARTINEZ-MARTIN¹, Fernando GONZALEZ-VIDOSA²,
 Antonio HOSPITALER², Víctor YEPES^{†‡2}

⁽¹⁾Department of Geotechnical Engineering, Universitat Politècnica de València, 46022 Valencia, Spain)

⁽²⁾Department of Construction Engineering, ICITECH, Universitat Politècnica de València, 46022 Valencia, Spain)

[†]E-mail: vyepesp@upv.es

Received Nov. 9, 2011; Revision accepted Feb. 23, 2012; Crosschecked May 15, 2012

Abstract: This paper describes one approach to the design of reinforced concrete (RC) bridge piers, using a three-hybrid multi-objective simulated annealing (SA) algorithm with a neighborhood move based on the mutation operator from the genetic algorithms (GAs), namely MOSAMO1, MOSAMO2 and MOSAMO3. The procedure is applied to three objective functions: the economic cost, the reinforcing steel congestion and the embedded CO₂ emissions. Additional results for a random walk and a descent local search multi-objective algorithm are presented. The evaluation of solutions follows the Spanish Code for structural concrete. The methodology was applied to a typical bridge pier of 23.97 m in height. This example involved 110 design variables. Results indicate that algorithm MOSAMO2 outperforms other algorithms regarding the definition of Pareto fronts. Further, the proposed procedure will help structural engineers to enhance their bridge pier designs.

Key words: Bridge piers, Concrete structures, Multi-objective optimization, Simulated annealing (SA), Structural design

doi:10.1631/jzus.A1100304

Document code: A

CLC number: TU37; TP391

1 Introduction

The traditional design of concrete structures concentrates on cost. However, other objectives, such as the embedded emissions of carbon dioxide, the consumption of energy and water, the constructability, the durability, amongst others, now attract research attention (Paya *et al.*, 2008; Paya-Zaforteza *et al.*, 2009; Yepes *et al.*, 2012). The emergence of personal computers in the 1980s indicated a turning point in the structural analysis, in particular with regard to the use of finite elements-based models. Other advances in the 1990s came with the use of the computer-aided design (CAD) tools, which significantly improved the structural designs. However, those design tools did

not, by themselves, optimize any structure, since structures were designed based on data supplied by users. The only way to achieve improvements in the CAD designs was to make several tests and reject those solutions that did not comply with any requirements imposed by the designer, in a trial-and-error process, where human-computer interaction is essential. Fortunately, optimization methods have provided an effective alternative to traditional-based design methods, where CAD-based software is included. However, we must not forget the importance of the designer experience, whose common sense is imperative to decide, ultimately, any proposed computer design.

The latest increase in heuristic optimization techniques is linked to artificial intelligence procedures. These approximate techniques are adequate for optimizing realistic structures because they provide good solutions at a reasonable computational cost. Much research has been conducted with regard to heuristic

[‡] Corresponding author

* Project supported by the Spanish Ministry of Science and Innovation (No. BIA2011-23602), and the European Community with the European Regional Development Fund (FEDER), Spain

© Zhejiang University and Springer-Verlag Berlin Heidelberg 2012

methods, such as genetic algorithms (GAs) (Holland, 1975), simulated annealing (SA) (Kirkpatrick *et al.*, 1983; Cerny, 1985), ant colony optimization (Dorigo *et al.*, 1996), particle swarm optimization (Kennedy and Eberhart, 1995; Zhang *et al.*, 2008), and harmony search optimization (Lee and Geem, 2004), *inter alia*. Heuristic optimization and other artificial intelligence procedures have been used with favorable outcome in different areas of structural engineering (Yepes and Medina, 2006; Ponz-Tienda *et al.*, 2012). Cohn and Dinovitzer (1994) conducted an extensive state-of-the-art study of the practical use of optimization in structural engineering. They brought out the gap between theoretical research and the practical applications, adding that mathematical optimization represents a high degree of complexity for the structural engineer and noting that most studies focused on steel structures, whereas only few dealt with concrete structures. The application of heuristic optimization to reinforced concrete (RC) structures began to appear in the late 1990s (Balling and Yao, 1997; Coello *et al.*, 1997). From then on, many studies based on evolutionary programming have been applied for optimizing structural concrete problems, especially GAs. Recently, other evolutionary algorithms have been developed for structural optimization, such as particle swarm optimization, ant colony optimization and harmony search (Kaveh and Talatahari, 2009; Khajehzadeh *et al.*, 2011). Kicinger *et al.* (2005) provided a review of evolutionary programming and structural design, while our research group has recently reported on non-evolutionary techniques for the CAD optimization of walls (Yepes *et al.*, 2008), frame bridges (Perea *et al.*, 2008), building frames (Paya-Zaforteza *et al.*, 2009), bridge piers (Martinez *et al.*, 2010), prestressed concrete precast pedestrian bridges (Marti and Gonzalez-Vidoso, 2010), and road vaults (Carbonell *et al.*, 2011). A review of multi-objective applications in structural engineering can be found in (Paya *et al.*, 2008).

The rectangular hollow section piers which are the object of this study are mainly used with heights of more than 20 m, and they are regarded as the most functional solution for the intermediate supports of viaducts. The external perimeter is usually embellished with relieves for decorative purposes (Fig. 1).

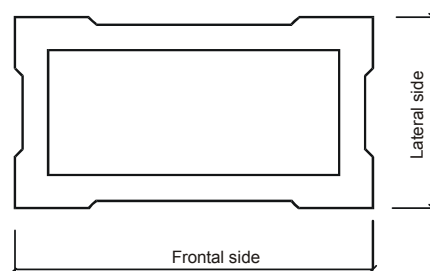


Fig. 1 Typical hollow cross-section of RC pier

Fig. 2 shows the parts of this pier: the foundation that is either a shallow footing or can include deep piles, the main hollow shaft and the top part that carries loads from the reactions of the pair of bridge bearings. The pier is built usually in stages of approximately 5 m in height. The footing foundation is designed in order to distribute the load on the supporting soil, whose dimensions depend on the permissible ground stress. Otherwise, pile foundation is required when ground strength is deficient. The main parameters that affect pier design are the pier height as well as the vertical and horizontal loads transferred from the deck and the permissible ground stress.

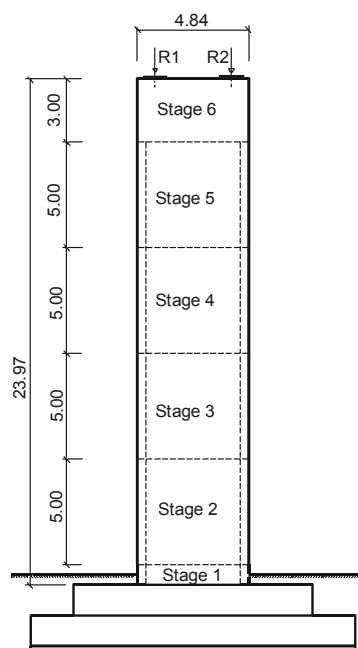


Fig. 2 Typical RC rectangular hollow section pier (unit: m)

Martinez *et al.* (2010) explored the single-objective cost optimization of this type of RC structure. In contrast, this paper concentrates on the fully multi-objective, hybrid-based SA optimization. The following methods consist of an evaluation computer module in which cross-section dimensions, materials and steel reinforcement are taken as discrete variables. This module computes the three objectives considered, i.e., the cost, the reinforcing steel congestion and the embedded CO₂ functions. Then, the module verifies whether a solution complies with all the applicable limit states. Multi-objective random search, local search and hybrid-based SA algorithms are then used to search the solution space.

2 Optimization problem definition

2.1 Cost function

Typically, in optimizing an RC structure, the objective is to minimize the cost of the structure and defined as

$$C = \sum_{i=1,r} p_i \cdot m_i(x_1, x_2, \dots, x_n), \quad (1)$$

where p_i is the unit price, m_i is the measurement of the unit in which the construction of the pier is split, and r is the total number of construction units. The cost function includes the price of materials (concrete and steel) and the formwork. The basic prices considered were taken from the BEDEC PR/CPT ITEC database (Catalonia Institute of Construction Technology, 2009) and are given in Tables 1–3. Note that a total of 56 concrete mixes are considered for the cost and the embedded CO₂ emissions. Concrete mix design takes into account the strength, the water/cement ratio and the slump. The slump is the number of centimeters that a conical frustum mix of concrete descends once the mould is removed. It is measured by an international test that is explained in (Neville, 1981). The concrete qualities can vary between the HA-25 and the HA-50 considered by the Spanish Concrete Code (Ministerio de Fomento, 2008), for example, HA-25(1) is the concrete type number 1 with 25 MPa of compressive cylinder strength at 28 d.

Table 1 Basic unit prices and embedded kg CO₂

Unit	Cost (€)	kg CO ₂
1 kg of steel of column (B500S)	1.09	2.82
1 kg of steel of foundation (B500S)	1.07	2.82
1 m ² of foundation formwork	18.19	14.55
1 m ² of exterior wall formwork	48.19	12.68
1 m ² of interior wall formwork	49.50	12.68
1 m ³ of column concrete placing (labour+pump)	26.03	31.00
1 m ³ of column concrete placing (labour+bucket)	27.34	–
1 m ³ of footing concrete placing (labour+bucket)	12.74	–
1 m ³ of earth removal	9.42	20.81
1 m ³ of earth fill-in	4.81	–

Table 2 Basic prices and kg CO₂ for concrete class 25 and 30 mixes

Unit (m ³)	Water/Cement	Cement (kg)	Slump	Cost (€)	kg CO ₂
HA-25(1)	0.65	250	Medium	70.79	224.34
HA-25(2)	0.60	275	Medium	72.78	244.94
HA-25(3)	0.60	300	Medium	73.93	265.28
HA-25(4)	0.60	325	Medium	75.49	285.62
HA-25(5)	0.60	350	Medium	76.63	305.97
HA-25(6)	0.65	250	Low	69.40	224.34
HA-25(7)	0.60	275	Low	71.35	244.94
HA-25(8)	0.60	300	Low	72.48	265.28
HA-25(9)	0.60	325	Low	74.01	285.62
HA-25(10)	0.60	350	Low	75.12	305.97
HA-30(1)	0.65	250	Medium	73.62	224.34
HA-30(2)	0.60	275	Medium	75.69	244.94
HA-30(3)	0.60	300	Medium	76.89	265.28
HA-30(4)	0.60	325	Medium	78.51	285.62
HA-30(5)	0.60	350	Medium	79.69	305.97
HA-30(6)	0.55	300	Medium	79.66	265.60
HA-30(7)	0.50	300	Medium	79.85	265.91
HA-30(8)	0.50	325	Medium	82.75	286.30
HA-30(9)	0.65	250	Low	72.18	224.34
HA-30(10)	0.60	275	Low	74.20	244.94
HA-30(11)	0.60	300	Low	75.38	265.28
HA-30(12)	0.60	325	Low	76.97	285.62
HA-30(13)	0.60	350	Low	78.13	305.97
HA-30(14)	0.55	300	Low	78.10	265.60
HA-30(15)	0.50	300	Low	78.29	265.91
HA-30(16)	0.50	325	Low	81.13	286.30

Table 3 Basic prices and kg CO₂ for concrete class 35, 40 and 45 mixes

Unit (m ³)	Water/ Cement	Cement (kg)	Slump	Cost (€)	kg CO ₂
HA-35(1)	0.65	250	Medium	76.45	224.34
HA-35(2)	0.60	275	Medium	78.60	244.94
HA-35(3)	0.60	300	Medium	79.85	265.28
HA-35(4)	0.60	325	Medium	81.53	285.62
HA-35(5)	0.60	350	Medium	82.76	305.97
HA-35(6)	0.55	300	Medium	82.80	265.60
HA-35(7)	0.50	300	Medium	82.92	265.91
HA-35(8)	0.50	325	Medium	85.93	286.30
HA-35(9)	0.45	350	Medium	88.72	307.06
HA-35(10)	0.65	250	Low	74.95	224.34
HA-35(11)	0.60	275	Low	77.06	244.94
HA-35(12)	0.60	300	Low	78.28	265.28
HA-35(13)	0.60	325	Low	79.93	285.62
HA-35(14)	0.60	350	Low	81.13	305.97
HA-35(15)	0.55	300	Low	81.20	265.60
HA-35(16)	0.50	300	Low	81.30	265.91
HA-35(17)	0.50	325	Low	84.25	286.30
HA-35(18)	0.45	350	Low	86.98	307.06
HA-40(1)	0.50	300	Medium	85.99	265.91
HA-40(2)	0.50	325	Medium	89.12	286.30
HA-40(3)	0.45	350	Medium	92.00	307.06
HA-40(4)	0.50	300	Low	84.31	265.91
HA-40(5)	0.50	325	Low	87.37	286.30
HA-40(6)	0.45	350	Low	90.20	307.06
HA-45(1)	0.50	300	Medium	89.07	265.91
HA-45(2)	0.50	325	Medium	92.30	286.30
HA-45(3)	0.45	350	Medium	92.00	307.06
HA-45(4)	0.50	300	Low	87.32	265.91
HA-45(5)	0.50	325	Low	90.49	286.30
HA-45(6)	0.45	350	Low	93.42	307.06

2.2 Reinforcing steel congestion function

Apart from the cost function, two other objective functions are considered. The economy of cast-in-place RC structures depends largely on decisions made early in advance in regards to framing dimensions, repetition and clearness of formwork. To this end, the first additional function is based on the number of bars of the structure, which was originally proposed by Koumouis *et al.* (1996). It may be argued that optimization based only on cost often results in structures whose constructability is poorly treated, since results tend to arrangements with too many different diameters and narrowly spaced small diameter bars. In this sense, the number of bars is

regarded as an indicator of reinforcing steel congestion, for fewer bars imply larger diameters with greater spacing. Moreover, fewer bars imply fewer execution errors, less complex quality controls and faster construction processes. The present study caters to constructability by using practical reinforcement arrangements and ensuring that bar spacing satisfies minimum distances in the code of practice. The second objective function is the total number of bars in the structure, N_b , i.e.,

$$N_b = \sum_{\text{Column}} (n_B + n_{CL} + n_{CT}) + \sum_{\text{Foundation}} n_F, \quad (2)$$

where n_B , n_{CL} and n_{CT} are the number of bars on the top block, the number of longitudinal bars in the hollow column, and the number of transverse bars in the hollow column, respectively, and n_F is the number of bars in the foundation.

2.3 CO₂ objective function

The CO₂ objective function quantifies the total amount of carbon dioxide emissions resulting from the use of materials which involves emissions at different stages of production, transportation, and placement. As a general rule, the higher the cost, the lower its sustainability. Different structural alternatives may be assessed and compared from an environmental viewpoint. The present study proposes a CO₂-environmental function to analyze bridge piers which is expressed as follows:

$$E = \sum_{i=1,r} e_i \cdot m_i(x_1, x_2, \dots, x_n), \quad (3)$$

where e_i is the CO₂ unit emission from the bridge pier material. The values of e_i for concrete, steel and formwork in the present study were obtained from the BEDEC database (Catalonia Institute of Construction Technology, 2009) and are specified in Tables 1–3. The bounds and scope of CO₂ emissions modeling include (1) the extraction of raw materials, (2) the transportation of raw materials to the factory, (3) the processing, manufacturing and fabrication of products and machinery, and (4) the emissions equipment involved in the construction processes in order to execute the structural work units. Despite the importance of transporting materials to the construction site, neither the use/maintenance nor the removal/disposal

phases for long-lived RC structures are considered in the BEDEC database, which are highly dependent in all case studies.

2.4 Problem definition

The proposed framework for the optimization of concrete structures involves a fully multi-objective optimization of the cost, the reinforcing steel congestion and the embedded CO₂ emissions of the structure. Note that multi-objective optimization techniques can deal with many objectives at the same time and this study will work with the three objective functions together. In these terms, this multi-objective optimization aims to minimize the objective functions f_1 , f_2 and f_3 of Eqs. (4)–(6) while satisfying the constraints of Eq. (7).

$$C = f_1(x_1, x_2, \dots, x_n), \quad (4)$$

$$N_b = f_2(x_1, x_2, \dots, x_n), \quad (5)$$

$$E = f_3(x_1, x_2, \dots, x_n), \quad (6)$$

$$g_j(x_1, x_2, \dots, x_n) \leq 0. \quad (7)$$

Note that the objective function f_1 in Eq. (4) is the cost of the structure expressed as the sum of unit prices multiplied by the measurements of construction units (Section 2.1). In addition, f_2 and f_3 are the second and third objective functions, i.e., specific measurements of the reinforcing steel congestion of the structure (Section 2.2) and the embedded CO₂ emissions (Section 2.3). For nontrivial multi-objective problems, there is no solution that simultaneously minimizes all objective functions since the objective functions are in conflict. This leads to the concept of Pareto optimality (Deb, 2001). A solution is said to belong to the Pareto set when there is no other solution overshadowing it in the graph f_1 vs. f_2 or f_3 . A set of inequality constraints g_j in Eq. (7) are all the serviceability limit states (SLSs) and ultimate limit states (ULSs) that the structure must be satisfied, as well as the geometry and constructability constraints of the problem (Section 2.5). The design variables are described together with the parameters of the problem as the design representation space (Section 2.6).

2.5 Problem constraints

Eq. (4) represents the entire limit states in which, when exceeded, it may be considered that the struc-

ture does not accomplish one of the functions that has been designed. The structural constraints for bridge piers have been fully discussed in a previous study (Martinez *et al.*, 2010). The column must comply with the ULSs for buckling, shear and fatigue, and the SLS for cracking. The ULS for buckling requires the greatest amount of computing time. Reinforcing steel is checked against flexure, shear, cracking and fatigue. The SLS verification of the footing involves checking whether the ground has sufficient bearing resistance to bear to the actions. It is assumed that the stresses under the footing are linearly distributed. A triangular distribution is used in the case of lifting and a trapezoidal block otherwise. As an additional check, the minimum amount of steel reinforcement due to flexural, shear and geometry is verified as prescribed by the Spanish Concrete Code (Ministerio de Fomento, 2008).

Apart from the explicit restrictions, such as structural constraints, the problem includes implicit constraints regarding the geometry, the materials and the constructability of solutions. Inter alia, these implicit constraints contain the choice of a hollow section, the set of bar diameters, the reinforcement setup, the maximum and minimum thickness values of the walls, etc.

2.6 Design variables and parameters

The design variables x_1, x_2, \dots, x_n can be varied without restriction to define a solution, whilst the parameters are all the magnitudes taken as fixed data. The number of column building stages determines the number of design variables. This study considers six column stages as shown in Fig. 2. The total number of variables in the present study is 110, which differs from a previous model where the number of variables was 95 (Martinez *et al.*, 2010). The differences between them are due mainly to the present treatment of concrete mixes for the required computation of embedded CO₂ emissions. All variables are discrete in the present model.

The total number of variables for the column is 91, where the first 24 variables define the sequence of concrete materials. There are four variables for each of the six column stages in Fig. 2, which are the compressive concrete strength, the water/cement ratio, the mass of cement of the mix and the slump. The only constraint of these variables is that the

compressive strength has to reduce with height, i.e., the compressive strength of a column stage has been always equal or lower than that in the stage below. Concrete strength can vary from 25 to 45 MPa in steps of 5 MPa, the water/cement ratio can vary from 0.45 to 0.65 in steps of 0.05, and the cement content can vary from 250 to 350 kg/m³ in steps of 25 kg/m³. Placing of concrete has two options: pumping of concrete with a medium slump and placing with a bucket with a low slump. All feasible combinations of strength and concrete mix are detailed in Tables 2 and 3. The next 10 variables define the front and lateral wall thickness of the five hollow sections in Fig. 2. Additionally, the remaining 57 variables define the reinforcing steel. The first two variables for the steel define the steel inner and outer covers, which are constant for the whole height of the pier. The longitudinal reinforcing steel is defined by 40 variables. The bar diameters and the number of the bars determine the longitudinal reinforcing set up, which is in the inner and outer faces of the lateral and frontal sides of the five hollow sections of the pier. Nominal bar diameters considered are 12, 16, 20, 25 and 32 mm and spacing varies from 0.10 to 0.30 m in steps of 0.02 m. As in construction practice, the reinforcement steel can only be reduced in height. The last 15 variables have been designed at the ULS of failure due to shear stresses. The tables of reinforcement include bar diameters and spacing, so all the ULSs and SLSs can be checked in detail.

The footing is defined with 19 variables. The first five ones are geometrical and define the total depth of the footing, the rectangular footing and the plinth plan dimensions. The depth of the footing measures between 1.00 and 4.00 m in steps of 0.10 m, and the plan dimensions of the footing vary between 8.00 and 15.00 m in steps of 0.25 m. The depth of the plinth is equal to half the total depth of the footing, whereas the plan dimensions of the plinth range from 4.00 to 15.00 m in steps of 0.25 m. Three variables characterize the grade of concrete, the cement content and the water/cement ratio in the dosage. Lastly, the 11 remaining variables determine the cover and the footing and plinth reinforcement.

The main parameters can be grouped as geometrical, ground properties, design actions, partial safety factors and durability requirements. As mentioned above, the pier height is 23.97 m, the frontal

side of the cross-section of the pier is 4.84 m, and the lateral dimension is fixed at 2.60 m as in the built pier. The actions considered together with the main parameters are summarized in Table 4. These parameters are kept constant for the calibration of the algorithms described in Section 4.

Table 4 Basic parameters of geometry and actions of the pier

Parameter	Value
Transverse dimension of the pier (m)	4.84
Longitudinal dimension of the pier (m)	2.60
Height of pier (m)	23.97
Height of top end block (m)	3.00
Height of formwork stage (m)	5.00
Number of bearings	2
Spacing of bearings (m)	3.60
Transverse dimension of bearing (m)	1.20
Longitudinal dimension of bearing (m)	1.20
Earth fill density (kN/m ³)	20.00
Permissible ground stress (kN/m ²)	500.00
Maximum load SLS of reactions R_1, R_2 (kN)	15445, 14241
Maximum torque SLS of reactions R_1, R_2 (kN)	15690, 11442
Minimum load SLS of reactions R_1, R_2 (kN)	11724, 11708
Bearing deformation force (kN)	725.25
Braking horizontal force (kN)	262.12
Wind horizontal force (kN)	1503.77

3 Multi-objective optimization procedures

The five multi-objective heuristic search methods are the random search (RS), the descent local search (DLS) and three versions of the SA method. Additionally, a single-objective version of the SA algorithm is also considered to assess the quality of the Pareto results when compared to single-objective results. Note that the RS has no intelligence on how to approach the optimal point or on how to construct the Pareto front in the case of multi-objective optimization. However, it was included since it allows an estimation of the correlation of the objective functions.

3.1 Multi-objective random search

The first multi-objective method used is the random search, which consists of generating solutions by random choice of the optimization problem

variables. The objective functions of each random solution are evaluated as well as the structural constraints to check whether the solution is feasible or not. This direct-search and iterative algorithm has no intelligence, but it is worth looking at the solution space and to estimate the proportion of feasible solutions from the total number of generated solutions. Additionally, the multi-objective RS allows a first estimation of the Pareto fronts and also allows for estimating the correlation of different objective functions. Furthermore, providing random initial solutions is useful as the starting point of other heuristics. Results for 50000 feasible iterations will be presented in Section 4.

3.2 Multi-objective descent local search

The multi-objective DLS is a hill climbing search, iterative and trajectory method that starts with a random solution, and then modifies this solution by an appropriate move mechanism. Here, a mutation operator from GAs was chosen as the moving mechanism, based on a small random perturbation to the values of some of the variables that define the current solution. The present algorithm changes at random 21 variables for the column and five for the footing, which is about 25% of the total number of variables. Changes are one position up or down the current value of each of the variables. Single-objective DLS accepts a candidate new solution when it fulfills the structural constraints and improves the objective function. In the present analysis, there are three objective functions and the analysis searches the Pareto 3D surface of the multi-objective problem. Therefore, there are three possible cases for any new trial solutions that satisfy the structural constraints. The first case is that the new candidate solution is dominated by any of the solutions in the Pareto surface, which implies that this candidate solution is ignored. The second case occurs when the candidate solution overshadows one or several of the solutions in the Pareto surface, which implies that the new candidate solution replaces those overshadowed solutions in the Pareto surface. The third possibility is that it neither overshadows solutions of the Pareto surface nor it is overshadowed, which implies that the candidate solution is inserted in the Pareto surface. The algorithm is run a number of times to generate different solutions. Each run starts with a random solution and lasts 10000 acceptances or 1000 itera-

tions without improvement. The Pareto surface is updated after each run. The algorithm stops after 10 runs without improvement of the Pareto surface with a maximum of 1000 runs.

3.3 Single-objective hybrid SA algorithm with mutation operator

The single-objective SA was independently described by Kirkpatrick *et al.* (1983) and Cerny (1985) and is the basis of the multi-objective optimization algorithm of Section 3.4. Annealing is a physical process often performed to relax the system to a state with minimum free energy. Based on the annealing process in statistical mechanics, SA simulates the process endured by wrongly positioned atoms in a metal when is heated and then slowly cooled under controlled conditions. At high temperatures, the atoms move freely with respect to one another. Nevertheless, if the mass is cooled slowly, thermal mobility is lost. SA applies a stochastic acceptance criterion to accept new solutions according to the expression $\exp(-\Delta f/T)$, where Δf is the deterioration in the optimization function and T is the temperature (a positive control parameter). The new current solution is accepted when a random number uniformly distributed in the interval (0, 1) is smaller than $\exp(-\Delta f/T)$. A predefined number of iterations, called Markov chains, are allowed while keeping the temperature fixed. The temperature is lowered very slightly according to a cooling schedule, in this way SA is capable of surpassing local optima at high-medium temperatures and gradually converges as the temperature reduces to zero. SA requires selecting the initial temperature, the length of the Markov chains and the cooling scheme, which can have a significant impact on the effectiveness of the algorithm. The initial temperature considered is given as

$$T_0 = \frac{\sum_{i=1, n_v} \Delta f}{n_v \ln(p_0^{-1})}, \quad (8)$$

where p_0 is the initial probability and n_v is the number of solutions that worsen the objective function.

From another standpoint, GAs are adaptive search procedures based on the process of natural evolution, which explore the search space using a population of solutions and operators such as selection,

crossover and mutation (Holland, 1975). In general, GA produces diversified solutions but shows poor convergence properties, which may not be able to explore the whole solution space without a fitting neighborhood structure. Some studies (Wong, 2001; Soke and Bingul, 2006) implemented a hybrid methodology in order to combine the synergy between the GA and SA and obtained hopeful results. The idea is to employ SA with a neighborhood move based on the GA mutation operator (Wu *et al.*, 2009).

The method in this study is a hybrid SA algorithm with a mutation operator (SAMO), which starts with a random solution. After several experiments, the mutation proposed was a random variation of 25% of the variables. Mutation was based on a small random perturbation to the values of some of the variables that define the current solution. These small random variations were selected to avoid a totally random search in the solution space, and they are justified for practical and constructive processes. The subset of solutions that worsen the objective function has n_v solutions, which are used to compute their average Δf in Eq. (8). The value of the initial probability (p_0) was adjusted to 0.7 in order to obtain high initial temperatures that improve the exploration part of the algorithm. The length of the Markov chains was 2000 iterations. Regarding the cooling scheme, a geometrical decrease was considered with a coefficient of 0.95. The procedure reduces the temperature when the number of iterations achieves the Markov chain length or when the number of acceptances is larger than 10% of the chain length. The stop criterion requires that the temperature is lower than the initial temperature divided by 1000000 and there are no acceptances in the whole Markov chain.

3.4 Multi-objective hybrid SA algorithm with mutation operator

The first multi-objective SA algorithm was proposed by Serafini (1992). More recent developments of the method were undertaken by Suppaitnarm *et al.* (2000). A good overview of multi-objective SA approaches can be found in (Bandyopadhyay *et al.*, 2008). Three different multi-objective algorithms based on a hybrid SA algorithm with a mutation operator (MOSAMO) are developed for the present study, namely MOSAMO1, MOSAMO2 and MOSAMO3. These algorithms differ in the initial

temperature and the probabilistic transition rule. Similar to the single-objective SAMO, the cooling scheme follows a geometrical decrease with a coefficient of 0.95. Further, the procedure reduces the temperature when the number of iterations achieves the Markov chain length of 2000, or when the number of acceptances is larger than 10% of the chain length. The stop criterion requires that the temperature is lower than the initial temperature divided by 1000000, and there are no acceptances in the whole Markov chain. The algorithm is run a number of times. The algorithm stops after 10 runs without improvement of the Pareto surface with a maximum of 1000 runs. This stop criterion led to 322 runs for MOSAMO1, 455 for MOSAMO2 and 255 for MOSAMO3. Fig. 3 shows a flowchart of the simulated process.

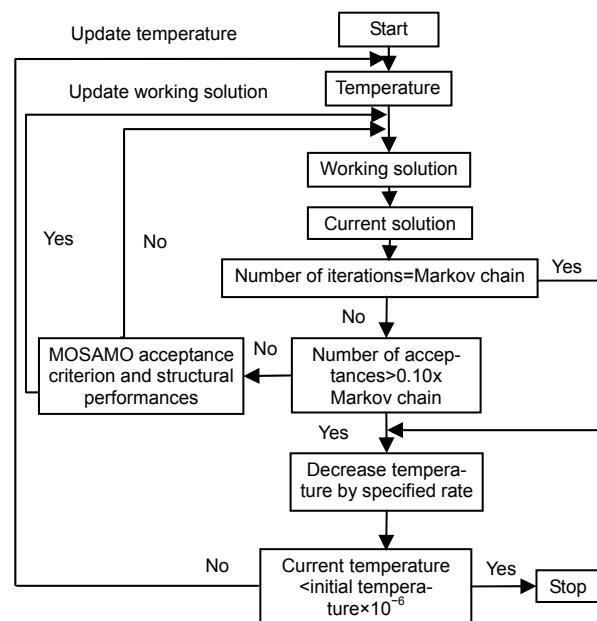


Fig. 3 Flowchart of the simulated process

The initial temperature for MOSAMO1 is given as

$$T_{0k} = \frac{\sum_{i=1, n_k} \Delta f_{ki}}{n_{vk} \ln(p_{ok}^{-1})}, \quad (9)$$

where p_{ok} is the initial probability and n_{vk} is the number of solutions that worsen the k th objective function.

Note that the initial temperature is different for each of the three objective functions. As for the single-objective SAMO, the algorithm starts with a random solution. The procedure then generates a mutation consisting of a random variation of 25% of the variables. The subset of solutions that worsen the different objective function has n_{vk} solutions, which are used to compute their average Δf_k in Eq. (9). p_{ok} is taken as 0.7 for the three objective functions to have high initial temperatures. Smaller values would shorten the search but restrict too much the acceptance conditions in the initial stages of the search. Larger values would unnecessarily delay the search.

The probability transition rule considered for MOSAMO1 is given as

$$p = \prod_{k=1}^m \sqrt[m]{e^{-\Delta f_k / T_k}} \tag{10}$$

A candidate solution will be accepted when a random number between 0 and 1 is smaller than the probability given by Eq. (10). The value of m is equal to the three objective functions considered.

The initial temperature considered for MOSAMO2 is

$$T_{0k} = \frac{\sum_{i=1, n_{vk}} \Delta f_{ki}}{\alpha_k n_{vk} \ln(p_{ok}^{-1})} \tag{11}$$

$$\alpha_k = \frac{r_k}{\sum_{j=1, m} r_j} \tag{12}$$

where α_k is the weight of the k th objective function under the Suppaitnarm *et al.* (2000) criteria, and r_j is random number between 0 and 1. The sum of the three α_k is equal to 1. α_k weights can be interpreted as a common initial transition probability for all objective functions. For each annealing process, a set of α_k is randomly generated to perform a multidirectional search along the Pareto frontier.

The probability transition rule considered for MOSAMO2 is

$$p = \prod_{k=1}^m \sqrt[1/\alpha_k]{e^{-\Delta f_k / T_k}} \tag{13}$$

Similar to MOSAMO1, a candidate solution will be accepted when a random number between 0 and 1 is smaller than the probability given by Eq. (13).

MOSAMO3 has an initial temperature common to the three objective functions:

$$T_0 = \frac{\sum_{k=1, m} \left(\frac{1/n_{vk} \sum_{i=1, n_{vk}} \Delta f_{ki}}{\ln(p_0^{-1})} \right)}{\ln(p_0^{-1})} \tag{14}$$

The values in Eq. (14) are as those explained for MOSAMO1 and MOSAMO2 algorithms. Finally, the probability transition rule considered for MOSAMO3 is

$$p = \prod_{k=1}^m \sqrt[m]{e^{-\Delta f_k / T}} \tag{15}$$

4 Numerical experimental results

The algorithms were programmed in Fortran Compaq Visual Professional Edition 6.6.0. Computer runs were performed using a conventional PC computer with an Intel Corel 2 CPU of 3.00 GHz and 2 GB of RAM. Firstly, a random search was performed with 50000 iterations to study relations between the three objective functions, which lasted 73750 s. The percentages of feasible solutions for the column and the footing are 0.13% and 0.12%, respectively. This means that only about one in a thousand randomly generated solutions are feasible. Fig. 4 depicts the relation between cost and the number of bars. The low correlation factor of $R^2=0.3421$ indicates that the functions are quite independent.

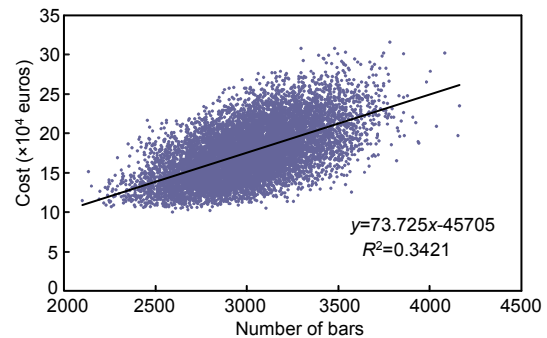


Fig. 4 RS cost vs. number of bars

Similarly, Fig. 5 shows the relation between cost and CO₂ emissions. In this case, the correlation factor of $R^2=0.9921$ is high and indicates an almost linear relation between the two objective functions.

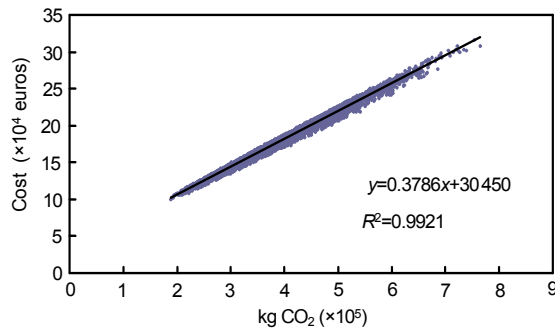


Fig. 5 RS cost vs. kg CO₂

Thirdly, Fig. 6 depicts the relation between the number of bars and CO₂ emissions. Again, the low correlation factor of $R^2=0.3347$ indicates that the functions are quite independent.

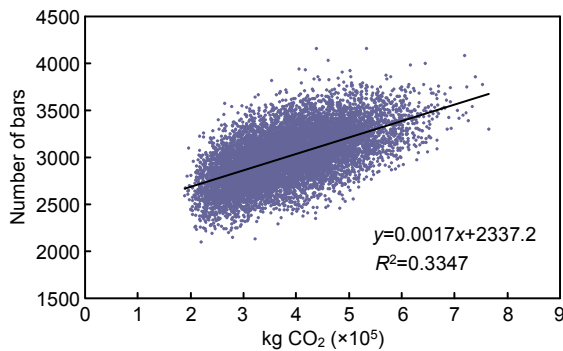


Fig. 6 RS number of bars vs. kg CO₂

The average computer times required for DLS, SAMO, MOSAMO1, MOSAMO2 and MOSAMO3 algorithms were 329, 1656, 335, 1456 and 787 s, respectively. Tables 5–7 summarize the main numerical results for all the algorithms used, where Table 5 is for the best cost solutions, Table 6 for the best CO₂ emissions, and Table 7 for the best number of bars solutions. These values show the extreme values of the Pareto surface.

Table 5 indicates that the MOSAMO2 solution of $C=88186.27$ euros is only 0.01% higher than the best single-objective SAMO solution of $C=88177.38$ euros. Moreover, DLS, MOSAMO1 and MOSAMO3 solutions are 0.23%, 1.11% and 0.2% higher than the SAMO solution, respectively. Similarly, Table 6 indi-

cates that the MOSAMO2 solution of CO₂=149030.33 kg CO₂ is only 0.2% higher than the best single-objective SAMO solution of CO₂=148736.77 kg CO₂. Otherwise, DLS, MOSAMO1 and MOSAMO3 solutions are 0.46%, 0.76% and 0.64% higher than the SA solution, respectively. Finally, Table 7 indicates that the MOSAMO2 solution of $N_b=1628$ is as good as the single-objective solution. The cost of this MOSAMO2 solution is $C=99385.74$ euros, which is 12.71% more than the best cost SAMO solution with a reduction of 66.83% in the number of bars.

Table 5 Summary of best cost algorithm results

Algorithm	Cost (€)	kg CO ₂	N_b
RS	99 105.63	182 542.62	2958
DLS	88 382.37	150 781.38	2970
MOSAMO1	89 159.37	152 644.91	2886
MOSAMO2	88 186.27	150 389.83	2853
MOSAMO3	88 534.00	151 148.52	3082
SAMO	88 177.38	150 161.50	2716

Table 6 Summary of best kg CO₂ algorithm results

Algorithm	Cost (€)	kgCO ₂	N_b
RS	99 105.63	182 542.62	2958
DLS	89 278.78	149 426.61	2830
MOSAMO1	89 566.13	149 868.19	2636
MOSAMO2	89 342.74	149 030.33	2792
MOSAMO3	90 081.89	149 691.92	2760
SAMO	89 440.99	148 736.77	2679

Table 7 Summary of best N_b algorithm results

Algorithm	Cost (€)	kgCO ₂	N_b
RS	104 628.33	190 049.45	2409
DLS	102 185.00	190 176.39	1628
MOSAMO1	103 448.81	190 176.25	1693
MOSAMO2	99 385.74	184 292.53	1628
MOSAMO3	98 005.38	180 864.38	1679
SAMO	106 340.39	203 508.20	1628

Fig. 7 shows a projection of the Pareto surface on the plane N_b -kg CO₂. Similarly, Fig. 8 shows a projection of the Pareto surface on the plane N_b -cost. These two figures include results for the DLS, MOSAMO1, MOSAMO2 and MOSAMO3 algorithms.

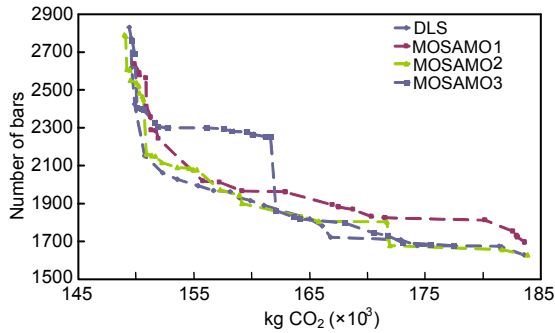


Fig. 7 Pareto front number of bars vs. kg CO₂

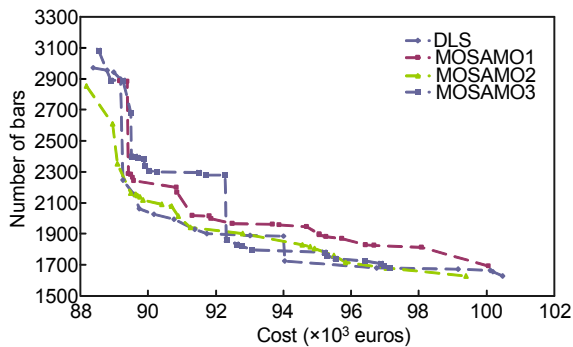


Fig. 8 Pareto front number of bars vs. cost

The best algorithms for the Pareto front N_b -kgCO₂ in Fig. 7 are the DLS and the MOSAMO2. Regarding the Pareto front N_b -cost, the best algorithms are DLS, MOSAMO1 and MOSAMO2 for low cost solutions and the DLS, MOSAMO2 and MOSAMO3 for high cost solutions. In general terms, it appears that the algorithm MOSAMO2 is the best algorithm regarding the definition of Pareto fronts, although the running times are about three times larger than those for algorithms MOSAMO1 and MOSAMO3. Note that the cost-kg CO₂ front is not relevant because of the functional relation between the two objective functions.

Figs. 9–11 show the bottom-section of the pier for the MOSAMO2 best cost, best N_b and best CO₂ solutions, respectively.

Finally, Fig. 12 shows the bottom section of the best Pareto distance solution. This is the solution that minimizes the distance of the Pareto surface to the Pareto utopia, which is the point with function coordinates equal to the minimum values obtained for the three objective functions. The cost of this solution is 88 186 euros, the amount of CO₂ is 149 030 kg and the number of bars is 2609.

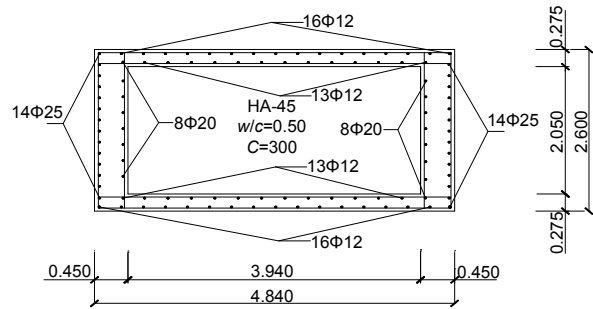


Fig. 9 Bottom section best MOSAMO2 cost result (unit: m)

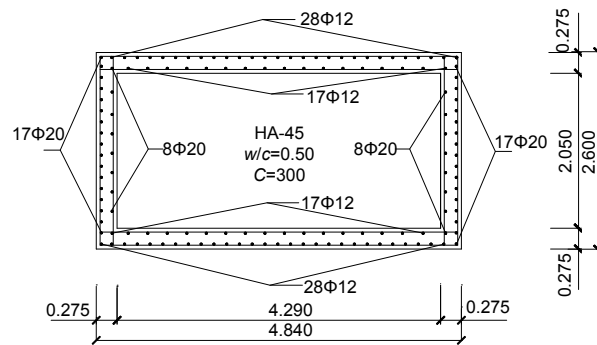


Fig. 10 Bottom section best MOSAMO2 kg CO₂ result (unit: m)

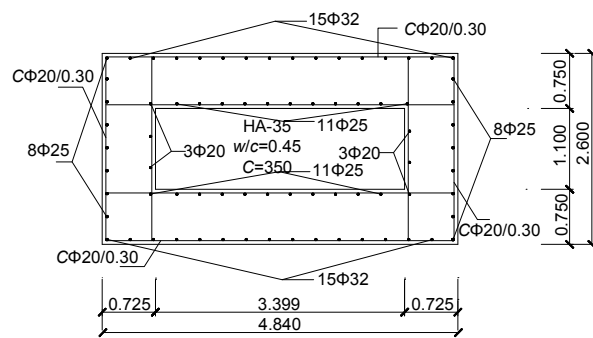


Fig. 11 Bottom section best MOSAMO2 N_b result (unit: m)

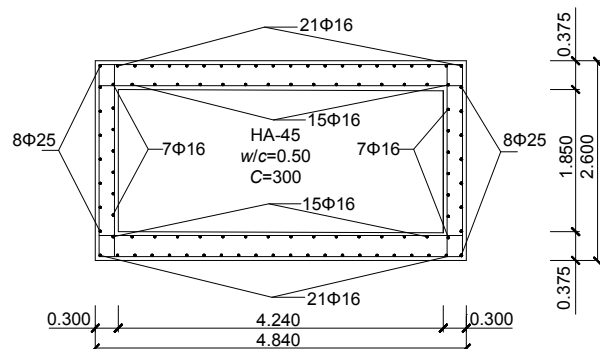


Fig. 12 Bottom section best distance multi-objective result (unit: m)

5 Conclusions

Five multi-objective algorithms for the design of rectangular hollow section piers are described, i.e., RS, DLS, MOSAMO1, MOSAMO2 and MOSAMO3. The three versions of the multi-objective SA proposed differ in the formulation of the initial temperature and the probability transition rule to accept worsening solutions. Three objective functions were considered, namely the cost, the number of bars in the structure and the amount of embedded CO₂ emissions. First, a random search was executed to study the correlation of the three objective functions. It was concluded that the relation between cost and embedded CO₂ was almost functional. Conversely, it was observed that the correlation of the number of bars with either the cost or the embedded CO₂ was very low. The comparison between the results indicates that best DLS and MOSAMO1-MOSAMO2-MOSAMO3 results are close to SAMO single-objective results. This leads to the conclusion that the multi-objective algorithms are well calibrated and accurate. Although both the DLS and the three MOSAMO Pareto results were satisfactory, it is worth noting that the best Pareto front results were obtained with the algorithm MOSAMO2, which includes weights α_k for the initial temperature and the transition rule. These weights selectively stimulate the search in the direction of any of the three objective functions. Note that the algorithm restarts until no improvement in the Pareto front is detected in 10 runs, so the use of weights improves the quality of the solutions. In addition, this paper includes in the objective functions the variables that account for concrete mixing. This allows the prediction of the optimum solution together with the concrete mix and the procedure for concrete placing. The study gives a new state-of-the-art heuristic for the multi-objective optimized design of RC structures. The RS-DLS-MOSAMO sequence is applied successfully to the detailed design of a 110-design variables bridge pier of 23.97 m in height. This study corroborates that the economic optimization has a high correlation to the embedded CO₂ optimization in the economic and technological context in which the piers are designed. In addition, this paper stresses that the reinforcing steel congestion objective and the cost/environmental objective are antagonist objectives, i.e., that constructability has cost and environ-

mental consequences. This is shown thanks to a detailed model that includes bar diameters and spacing in the design variables. Results lead to detailed drawings of the solutions.

References

- Balling, R.J., Yao, X., 1997. Optimization of reinforced concrete frames. *ASCE Journal of Structural Engineering*, **123**(2):193-202. [doi:10.1061/(ASCE)0733-9445(1997)123:2(193)]
- Bandyopadhyay, S., Saha, S., Maulik, U., Deb, K., 2008. A simulated annealing-based multi-objective optimization algorithm: AMOSA. *IEEE Transactions on Evolutionary Computation*, **12**(3):269-283. [doi:10.1109/TEVC.2007.900837]
- Carbonell, A., Gonzalez-Vidoso, F., Yepes, V., 2011. Design of reinforced concrete road vault underpasses by heuristic optimization. *Advances in Engineering Software*, **42**(4): 151-159. [doi:10.1016/j.advengsoft.2011.01.002]
- Catalonia Institute of Construction Technology, 2009. BEDEC PR/PCT ITEC Materials Database, Barcelona, Spain.
- Cerny, V., 1985. Thermodynamical approach to the traveling salesman problem: An efficient simulation algorithm. *Journal of Optimization Theory and Applications*, **45**(1): 41-51. [doi:10.1007/BF00940812]
- Coello, C.A., Christiansen, A.D., Santos, F., 1997. A simple genetic algorithm for the design of reinforced concrete beams. *Engineering with Computers*, **13**(4):185-196. [doi:10.1007/BF01200046]
- Cohn, M.Z., Dinovitzer, A.S., 1994. Application of structural optimization. *ASCE Journal of Structural Engineering*, **120**(2):617-649. [doi:10.1061/(ASCE)0733-9445(1994)120:2(617)]
- Deb, D., 2001. Multi-Objective Optimization Using Evolutionary Algorithms. Wiley, New York, USA.
- Dorigo, M., Maniezzo, V., Colomi, A., 1996. The ant system: optimization by a colony of cooperating agents. *IEEE Transactions on Systems, Man, and Cybernetics, Part B: Cybernetics*, **26**(1):29-41. [doi:10.1109/3477.484436]
- Holland, J.H., 1975. Adaptation in Natural and Artificial Systems. University of Michigan Press, Ann Arbor, USA.
- Kaveh, A., Talatahari, S., 2009. Particle swarm optimizer, ant colony strategy and harmony search scheme hybridized for optimization of truss structures. *Computers and Structures*, **87**(5-6):267-283. [doi:10.1016/j.compstruc.2009.01.003]
- Kennedy, J., Eberhart, R., 1995. Particle Swarm Optimization. IEEE International Conference on Neural Networks, Perth, Australia. IEEE Service Center, Piscataway, p.1942-1948.
- Khajehzadeh, M., Taha, M.R., El-Shafie, A., Eslami, M., 2011. Modified particle swarm optimization for optimum design of spread footing and retaining wall. *Journal of Zhejiang University-SCIENCE A (Applied Physics & Engineering)*, **12**(6):415-427. [doi:10.1631/jzus.A1000252]

- Kicinger, R., Arciszewski, T., de Jong, K., 2005. Evolutionary computation and structural design: A survey of the state-of-the-art. *Computers and Structures*, **83**(23-24): 1943-1978. [doi:10.1016/j.compstruc.2005.03.002]
- Kirkpatrick, S., Gelatt, C.D., Vecchi, M.P., 1983. Optimization by simulated annealing. *Science*, **220**(4598):671-680. [doi:10.1126/science.220.4598.671]
- Koumousis, V.K., Arsenis, S.J., Vasiloglou, V.B., 1996. Detailed design of reinforced concrete buildings using logic programming. *Advances in Engineering Software*, **25**(2-3):161-176. [doi:10.1016/0965-9978(95)00092-5]
- Lee, K.S., Geem, Z., 2004. A new structural optimization method based on the harmony search algorithm. *Computers & Structures*, **82**(9-10):781-798. [doi:10.1016/j.compstruc.2004.01.002]
- Marti, J.V., Gonzalez-Vidosa, F., 2010. Design of prestressed concrete precast pedestrian bridges by heuristic optimization. *Advances in Engineering Software*, **41**(7-8): 916-922. [doi:10.1016/j.advengsoft.2010.05.003]
- Martinez, F.J., Gonzalez-Vidosa, F., Hospitaler, A., Yepes, V., 2010. Heuristic optimization of RC bridge piers with rectangular hollow sections. *Computers and Structures*, **88**(5-6):375-386. [doi:10.1016/j.compstruc.2009.11.009]
- Ministerio de Fomento, 1998. IAP-98: Code on the Actions to be Considered for the Design of Road Bridges. Madrid, Spain (in Spanish).
- Ministerio de Fomento, 2008. EHE-08: Code of Structural Concrete. Madrid, Spain (in Spanish).
- Neville, A.M., 1981. Properties of Concrete, 3rd Edition. Pitman, London, UK.
- Paya, I., Yepes, V., Gonzalez-Vidosa, F., Hospitaler, A., 2008. Multi-objective optimization of concrete building frames by simulated annealing. *Computer-Aided Civil and Infrastructure Engineering*, **23**(8):596-610. [doi:10.1111/j.1467-8667.2008.00561.x]
- Paya-Zaforteza, I., Yepes, V., Hospitaler, A., Gonzalez-Vidosa, F., 2009. CO₂-optimization of reinforced concrete frames by simulated annealing. *Engineering Structures*, **31**(7): 1501-1508. [doi:10.1016/j.engstruct.2009.02.034]
- Perea, C., Alcalá, J., Yepes, V., González-Vidosa, F., Hospitaler, A., 2008. Design of reinforced concrete bridge frames by heuristic optimization. *Advances in Engineering Software*, **39**(8):676-688. [doi:10.1016/j.advengsoft.2007.07.007]
- Ponz-Tienda, J.L., Pellicer, E., Yepes, V., 2012. Complete fuzzy scheduling and fuzzy earned value management in construction projects. *Journal of Zhejiang University-SCIENCE A (Applied Physics & Engineering)*, **13**(1): 56-68. [doi:10.1631/jzus.A1100160]
- Serafini, P., 1992. Simulated Annealing for Multiple Objective Optimization Problems. Proceedings of the Tenth International Conference on Multiple Criteria Decision Making, Taipei, p.87-96.
- Soke, A., Bingul, Z., 2006. Hybrid genetic algorithm and simulated annealing for two-dimensional non-guillotine rectangular packing problems. *Engineering Applications of Artificial Intelligence*, **19**(5):557-567. [doi:10.1016/j.engappai.2005.12.003]
- Suppaitnarm, A., Seffen, K.A., Parks, G.T., Clarkson, P.J., 2000. A simulated annealing algorithm for multi-objective optimization. *Engineering Optimization*, **33**(1): 59-85. [doi:10.1080/03052150008940911]
- Wong, S.Y.W., 2001. Hybrid simulated annealing/genetic algorithm approach to short-term hydro-thermal scheduling with multiple thermal plants. *International Journal of Electrical Power & Energy Systems*, **23**(7):565-575. [doi:10.1016/S0142-0615(00)0029-6]
- Wu, T.H., Chung, S.H., Chang, C.C., 2009. Hybrid simulated annealing algorithm with mutation operator to the cell formation problem with alternative process routings. *Expert Systems with Applications*, **36**(2):3652-3661. [doi:10.1016/j.eswa.2008.02.060]
- Yepes, V., Medina, J.R., 2006. Economic heuristic optimization for the heterogeneous fleet VRPHESTW. *ASCE Journal of Transportation Engineering*, **132**(4):303-311. [doi:10.1061/(ASCE)0733-947X(2006)132:4(303)]
- Yepes, V., Alcalá, J., Perea, C., González-Vidosa, F., 2008. A parametric study of optimum earth-retaining walls by simulated annealing. *Engineering Structures*, **30**(3): 821-830. [doi:10.1016/j.engstruct.2007.05.023]
- Yepes, V., Gonzalez-Vidosa, F., Alcalá, J., Villalba, P., 2012. CO₂-optimization design of reinforced concrete retaining walls based on a VNS-threshold acceptance strategy. *ASCE Journal of Computing in Civil Engineering*, **26**(3): 378-386. [doi:10.1061/(ASCE)CP.1943-5487.0000140]
- Zhang, W.M., Li, S.J., Qian, F., 2008. θ -PSO: a new strategy of particle swarm optimization. *Journal of Zhejiang University-SCIENCE A*, **9**(6):786-790. [doi:10.1631/jzus.A071278]